



Electric-field-induced bound states and resonances in heteronuclear atomic collisions

Zi-Ang Li , Zi-Wei Wang, Gao-Ren Wang,^{*} and Shu-Lin Cong
School of Physics, Dalian University of Technology, Dalian 116024, China

 (Received 16 January 2020; revised manuscript received 23 March 2020; accepted 6 April 2020; published 6 May 2020)

The variations of the bound states of heteronuclear collision complexes in a static electric field are investigated. Using a prototype model, we engineer the interatomic interaction of the collision complex to have an l -wave bound state or quasibound state (virtual state for s wave) close to the threshold. The variation of such a state with electric field is calculated to find out whether it crosses the threshold and produces a zero-energy resonance. We identify the cases in which an electric-field-induced resonance can occur at low field. The prototype model is used to interpret the calculated results with realistic potentials for heteronuclear alkali-metal collision complexes. We also calculate the probability density of the low-energy scattering state and find that the short-range probability density can still be enhanced in the absence of electric-field-induced resonance.

DOI: [10.1103/PhysRevA.101.053409](https://doi.org/10.1103/PhysRevA.101.053409)

I. INTRODUCTION

Ultracold heteronuclear atomic gases have been widely investigated both experimentally and theoretically. They are ideal platforms for many intriguing applications such as preparation of ultracold polar molecules [1–5], investigation of few-body physics [6] and many-body physics [7–9], generation of quantum entanglement [10], and so on. The modulation of interatomic interaction plays an important role in all these applications.

The heteronuclear collision complex possesses permanent dipole moments at short-range interatomic distance and provides an opportunity to manipulate the interatomic interaction via the electric field. The electric field couples different partial waves and shifts the bound-state levels [11–16]. When a bound state or quasibound state crosses the threshold in the electric field, a zero-energy resonance is induced [17]. In the vicinity of electric-field-induced resonances, the short-range probability density of the low-energy scattering state is enhanced, and the photoassociation rate is increased [18,19]. Usually, an intensive electric field is required to induce a resonance. One intuitive way to reduce the strength of the electric field needed for the resonance is to choose the collision complexes with large permanent dipole moments, such as LiCs [14,15,18,19]. Another way is to manipulate the collision complexes in the vicinity of magnetic-field-induced Feshbach resonances or shape resonances [20–24]. In these cases, there are bound states or quasibound states [25] (virtual states for s waves [26]) close to the threshold in the absence of the electric field. The position of the field-free bound or quasibound(virtual) state is closely related to the electric field that induces the resonance.

In this work, we first study a prototype collision complex, the interatomic interaction of which is described by the Lennard-Jones (LJ) potential. The LJ potential is engineered

to support an l -wave bound or quasibound (virtual) state close to the threshold. We calculate the variation of the bound states with electric field and locate the zero-energy electric-field-induced resonance when a bound or quasibound (virtual) state crosses the threshold. Our aim is to identify the cases in which resonances are induced at low electric field. Then, we perform the calculation with a realistic potential of the ground electronic state for all the heteronuclear alkali-metal collision complexes and verify the observations obtained with the prototype system. We also calculate the probability density of the low-energy scattering state. It is found that the short-range probability density can still be enhanced in the absence of the electric-field-induced resonance.

This paper is organized as follows. In Sec. II, the theoretical model is described. In Sec. III, the results and discussion are given. A conclusion is drawn in Sec. IV.

II. THE THEORETICAL MODEL

Within the Born-Oppenheimer approximation, the relative motion Hamiltonian of two atoms in an electric field is given by

$$\hat{H} = -\frac{1}{2\mu R} \frac{\partial^2}{\partial R^2} R + \hat{V}_c(R) + \frac{\hat{l}^2}{2\mu R^2} + \hat{V}_\varepsilon(R), \quad (1)$$

where μ denotes the reduced mass and R denotes the internuclear distance. $\hat{V}_c(R)$ is the potential-energy operator, and \hat{l} is the partial-wave operator. The space-fixed z axis is chosen to be the direction of the applied electric field. $\hat{V}_\varepsilon(R)$ describes the interaction of the external electric field ε with the permanent electronic dipole moment $D(R)$ of the collision complex

$$\hat{V}_\varepsilon(R) = -\varepsilon D(R) \cos \theta, \quad (2)$$

where θ is the angle between the direction of the electric field and the direction of the dipole moment. We express the Hamiltonian (1) in the partial-wave basis $|lm\rangle$, where m is the magnetic quantum number and is conserved. The first

^{*}gaoren.wang@dlut.edu.cn

three terms on the right-hand side of Eq. (1) are diagonal in the partial-wave basis, while the last term couples different partial-wave states. The matrix elements of $\hat{V}_\varepsilon(R)$ are given by [18,21]

$$\langle lm|\hat{V}_\varepsilon(R)|l'm'\rangle = -\varepsilon D(R)\langle lm|\cos\theta|l'm'\rangle, \quad (3)$$

where

$$\begin{aligned} \langle lm|\cos\theta|l'm'\rangle &= \delta mm'(-1)^m \begin{pmatrix} l & 1 & l' \\ -m & 0 & m' \end{pmatrix} \begin{pmatrix} l & 1 & l' \\ 0 & 0 & 0 \end{pmatrix} \\ &\times [(2l+1)(2l'+1)]^{1/2}, \end{aligned} \quad (4)$$

and the large curved bracket stands for $3j$ symbol. In the low-electric-field region which we are interested in, the interaction of the atomic dipole polarizability with the electric field [27,28] is expected to be small and is omitted [16,18–21]. The effects of the interaction of atomic dipole polarizability with strong electric field on the bound and scattering states were studied in [27–30]. To obtain the energy and wave function of the bound states and scattering states for the collision complex in an electric field, we solve the stationary Schrödinger equation with Hamiltonian (1) using the mapped Fourier grid Hamiltonian method [31]. The lowest ten partial-wave states are included in the calculation to obtain convergent results.

III. RESULTS AND DISCUSSION

A. The bound states in the absence of electric field

First, we investigate the bound states of the collision complexes in the absence of electric field in order to introduce the connection between the scattering length and the least bound state [32]. In the vicinity of the threshold, one can adopt an effective potential instead of the realistic one to describe the bound states for the two-body system [33]. Here we use the LJ potential to describe the interatomic interaction

$$V_{\text{LJ}} = \frac{C_{10}}{R^{10}} - \frac{C_6}{R^6}, \quad (5)$$

where C_6 is the van der Waals coefficient and C_{10} is the parameter describing the short-range interaction.

For the LJ potential, one can analytically calculate the scattering length a and the energy E_l of the l -wave least bound level [34]. The reduced scattering length is denoted as $\tilde{a} = a/\beta_6$, and the reduced energy is $\tilde{E}_l = E_l/S_{E_6}$, where $\beta_6 = (2\mu C_6/\hbar^2)^{1/4}$ and $S_{E_6} = \hbar^2/2\mu\beta_6^2$ are the van der Waals length and energy scales, respectively. From the perspective of the quantum defect theory, the scattering length \tilde{a} and the energy \tilde{E}_l of the least bound level for the LJ potential equation (5) are determined by the dimensionless parameter $\tilde{\beta}_{10} = \beta_{10}/\beta_6$, where $\beta_{10} = (2\mu C_{10}/\hbar^2)^{1/8}$.

For a collision complex with an asymptotic van der Waals interaction, Gao indicated that the zero-energy bound states appear in sets [32]. If there is a zero-energy state of an l partial wave, there are also bound states of $l+4j$ ($l \geq 0$ and $j = 1, 2, \dots$) right at the threshold. Moreover, the l -wave zero-energy bound states appear when the reduced scattering length equals a specific value [32]. These are clearly seen in Fig. 1. The reduced scattering length \tilde{a} of the LJ

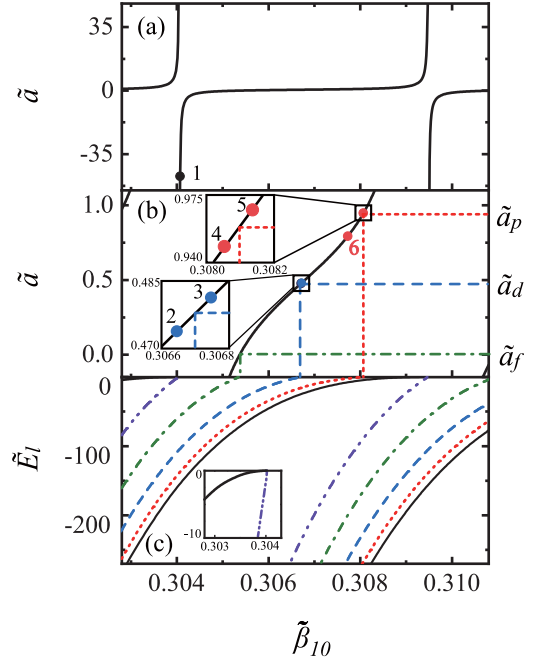


FIG. 1. (a) The scattering length \tilde{a} of the LJ potential as a function of the dimensionless parameter $\tilde{\beta}_{10}$. (b) An expanded view of \tilde{a} on the order of \tilde{a}_p , \tilde{a}_d , \tilde{a}_f , which are the p -wave, d -wave, and f -wave characteristic scattering lengths, respectively. (c) The energy \tilde{E}_l of the least bound state as a function of $\tilde{\beta}_{10}$ for $l = 0$ (black solid line), $l = 1$ (red dotted line), $l = 2$ (blue dashed line), $l = 3$ (green dot-dashed line), and $l = 4$ (purple double-dot-dashed line).

potential versus $\tilde{\beta}_{10}$ is shown in Fig. 1(a). The variation details of \tilde{a} in the range of $-0.15 < \tilde{a} < 1.10$ are shown in Fig. 1(b). The reduced energy \tilde{E}_l of the l -wave least bound state versus $\tilde{\beta}_{10}$ is shown in Fig. 1(c). There are both s -wave (black solid line) and g -wave (purple double-dot-dashed line) zero-energy bound states at $\tilde{\beta}_{10} = 0.304025$ [more clearly shown in the inset of Fig. 1(c)], and the corresponding scattering length equals $\tilde{a}_s \equiv \infty$, as shown in Fig. 1(a). Meanwhile f -wave (green dot-dashed line), d -wave (blue dashed line), and p -wave (red dotted line) zero-energy bound states appear at $\tilde{\beta}_{10} = 0.305383$, 0.306712 , and 0.308086 in Fig. 1(c), respectively. As shown in Fig. 1(b), the corresponding scattering length \tilde{a} equals characteristic scattering length $\tilde{a}_f \equiv 0$, $\tilde{a}_d \equiv 2\pi[\Gamma(1/4)]^{-2} \approx 0.47799$, and $\tilde{a}_p \equiv 4\pi[\Gamma(1/4)]^{-2} \approx 0.95598$, respectively [32].

In the following, we study the variation of the energy levels with electric field for a collision complex with an l -wave bound or quasibound (virtual) state close to the threshold. Utilizing the connection between the reduced scattering length \tilde{a} and reduced energy \tilde{E}_l of the least bound state, we select five cases, denoted by points 1–5 in Figs. 1(a) and 1(b). Specifically, there is an s -wave virtual state (point 1), p -wave bound and quasibound states (points 4 and 5, respectively), and d -wave bound and quasibound states (points 2 and 3, respectively) close to the threshold. The situations with an f and higher partial-wave bound or quasibound state are not considered since the resonances for $l \geq 3$ are difficult to observe in ultracold atomic gases due to the high centrifugal barrier [35].

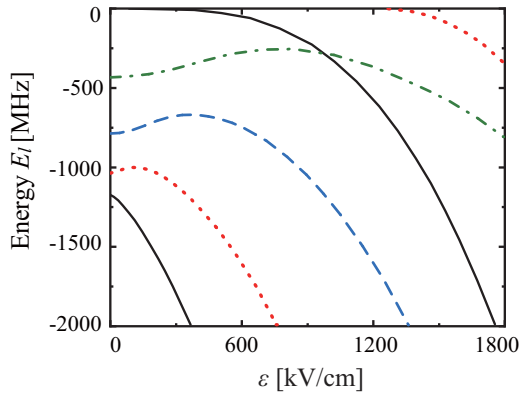


FIG. 2. The bound-state energy E_l as a function of the electric-field strength ε with $\tilde{\beta}_{10} = 0.304070$ and $\tilde{a} = -47.260$. The black solid line, red dotted line, blue dashed line, and green dot-dashed line correspond to $l = 0, 1, 2$, and 3 .

B. The bound states in electric field

In this section, a prototype model with $m = 0$ is studied, in which the interatomic interaction is described by the LJ potential. The reduced mass μ , the van der Waals coefficient $C_6 = 2686$ a.u. [36], and the permanent dipole moment $D(R)$ of the ground electronic state $X^1\Sigma^+$ [37] for $^{23}\text{Na}^{87}\text{Rb}$ are adopted. C_{10} and, correspondingly, $\tilde{\beta}_{10}$ are varied.

When $\tilde{\beta}_{10}$ is 0.304070 (point 1), the scattering length \tilde{a} is -47.260 , and there is an s -wave virtual state very close to the threshold at $\varepsilon = 0$ [26]. In Fig. 2 we show the variation of the bound state with electric field for this case. At $\varepsilon = 85$ kV/cm, the s -wave virtual state becomes a bound state, and a resonance takes place. As shown in Fig. 2, the energy of the s -wave bound state decreases monotonously with the increase of electric field. Hence, an s -wave bound state below the threshold at $\varepsilon = 0$ cannot produce a resonance in electric field.

As shown in Fig. 2, the energy of the p -wave (red dotted line) and d -wave (blue dashed line) bound states initially increases and then decreases as the electric field increases [38]. The critical electric field at which the bound-state energy reaches its maximum is larger for the d wave than for the p wave. Meanwhile, the increment of the bound-state energy at the critical electric field compared to the energy at $\varepsilon = 0$ is larger for the d wave than for the p wave. Different partial-wave states are coupled when the external electric field is applied. Nevertheless, Fig. 2 shows that each bound state at $\varepsilon \neq 0$ can be associated with a state described by quantum number l at $\varepsilon = 0$. Hence, we use l to label the bound states both at $\varepsilon = 0$ and $\varepsilon \neq 0$.

When $\tilde{\beta}_{10}$ is 0.306706 (point 2), \tilde{a} is 0.47647, which is slightly smaller than the d -wave characteristic scattering length \tilde{a}_d . In this case, there is a d -wave weakly bound state with $E_d = -0.5$ MHz at $\varepsilon = 0$, as shown in Fig. 3(a). As the external electric field is applied, this state becomes less bounded. It crosses the threshold at 260 kV/cm, and a resonance takes place. As the field strength gets stronger than 260 kV/cm, this bound state becomes a quasibound state. In Fig. 3(b), $\tilde{\beta}_{10}$ is 0.306717 (point 3), and \tilde{a} is 0.47954, which is slightly larger than \tilde{a}_d . By calculating the d -wave

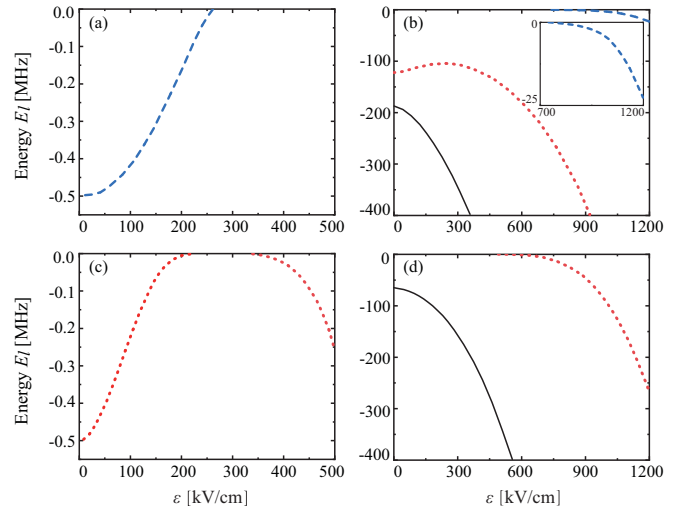


FIG. 3. The energy E_l as a function of electric-field strength ε for $l = 0$ (black solid line), $l = 1$ (red dotted line), and $l = 2$ (blue dashed line). In the absence of electric field, the collision complex has (a) a d -wave or (c) p -wave bound state with energy $E = -0.5$ MHz or (b) a d -wave or (d) p -wave quasibound state with energy $E = 0.5$ MHz.

cross section in the absence of the external electric field [34], a d -wave quasibound state is located at 0.5 MHz. With the increase of electric field, a resonance occurs at 740 kV/cm which is induced by the d -wave quasibound state crossing the threshold [see the inset of Fig 3(b)]. Comparing Figs. 3(a) and 3(b), we can see that a resonance takes place at lower electric field in the collision complex with a d -wave bound state close to the threshold at $\varepsilon = 0$.

When $\tilde{\beta}_{10}$ is 0.308064 (point 4), \tilde{a} is 0.94504, slightly smaller than the p -wave characteristic scattering length \tilde{a}_p . In this case there is a p -wave weakly bound state with $E_p = -0.5$ MHz at $\varepsilon = 0$, as shown in Fig. 3(c). This state crosses the threshold at 216 kV/cm, and a resonance is induced. As the field strength gets stronger than 216 kV/cm, this bound state becomes a p -wave quasibound state. As the electric field increases further, another scattering resonance appears at 339 kV/cm, which is caused by the p -wave quasibound state crossing back to the threshold. This can be understood by observing the change of the p -wave bound state with electric field, as shown in Fig. 2. When $\tilde{\beta}_{10}$ is 0.308107 (point 5), \tilde{a} is 0.96874, which is slightly larger than \tilde{a}_p . In this case, there is a p -wave quasibound state at $E_p = 0.5$ MHz [34]. In Fig. 3(d) we can see that a resonance appears at 494 kV/cm which is caused by the p -wave quasibound state crossing the threshold. Comparing Figs. 3(c) and 3(d), we can see that a resonance takes place at a lower electric field in the collision complex with a p -wave bound state close to the threshold at $\varepsilon = 0$.

The energies of the d -wave bound state in Fig. 3(a) and the p -wave bound state in Fig. 3(c) are the same at $\varepsilon = 0$. It is clearly shown that the p -wave bound state produces a resonance at lower electric field. Similarly, the energies of the d -wave quasibound state in Fig. 3(b) and p -wave quasibound state in Fig. 3(d) are the same at $\varepsilon = 0$, and the p -wave quasibound state produces a lower-field resonance. The p -wave and d -wave bound states should be quite close to the threshold

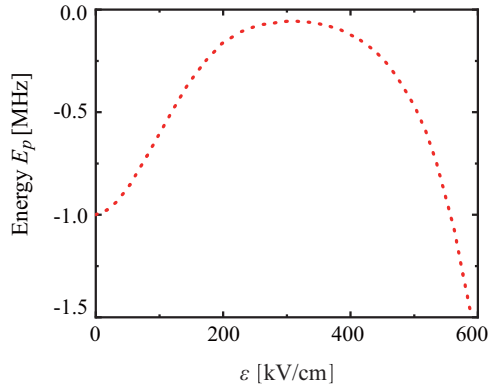


FIG. 4. The energy of the p -wave bound state E_p as a function of the electric-field strength ε in the collision complex having a p -wave bound state with $E_p = -1$ MHz at $\varepsilon = 0$.

so that they can cross the threshold in the electric field and produce resonances. Figure 4 shows the energy variation of the p -wave bound state with electric field for $\tilde{\beta}_{10} = 0.308045$ (point 6). For this case, there is a p -wave bound state with $E_p = -1$ MHz at $\varepsilon = 0$. As the electric field increases, this bound state moves towards the threshold but cannot cross the threshold. In the following, we show that, as this bound state gets close to the threshold, the short-range probability density of low-energy scattering states is enhanced.

C. Probability density of the low-energy scattering state

In the framework of the prototype model with $m = 0$, we now discuss the effect of the electric-field-induced resonance on the short-range probability density of the low-energy scattering state. We also investigate the effect on the low-energy scattering state caused by a bound state getting close to the threshold but never crossing it in the electric field. We choose the collision complexes with $\tilde{\beta}_{10} = 0.308064$ and 0.308045 as two examples.

For the collision complex with $\tilde{\beta}_{10} = 0.308064$ (point 4), there is a p -wave bound state with $E_p = -0.5$ MHz at $\varepsilon = 0$, and two resonances appear at $\varepsilon = 216$ and 339 kV/cm, as shown in Fig. 3(c). In the vicinity of these two resonances, the short-range probability density of the scattering state with the collision energy $E_{\text{col}} = 0.96 \mu\text{K}$ is enhanced by almost three orders, as shown in Fig. 5(a). Figures 5(b), 5(c) and 5(d) show the s -, p -, and d -wave components of the short-range probability density. One can see that the p -wave component is enhanced most significantly close to the resonances. This reflects the fact that the resonances are produced by the p -wave (quasi)bound states crossing the threshold.

For the collision complex with $\tilde{\beta}_{10} = 0.308045$ (point 6), there is a p -wave bound state with $E_p = -1$ MHz at $\varepsilon = 0$, and the energy variation of this p -wave state in the electric field is shown in Fig. 4. In Fig. 6, we show the contour plot of the short-range probability density of the scattering state at $E_{\text{col}} = 0.48 \mu\text{K}$ versus electric field and interatomic distance. One can see that the short-range probability density of the scattering state in Fig. 6 is enhanced when the p -wave bound state in Fig. 4 approaches the threshold. In order to show the enhancement effect more clearly, the short-range probability

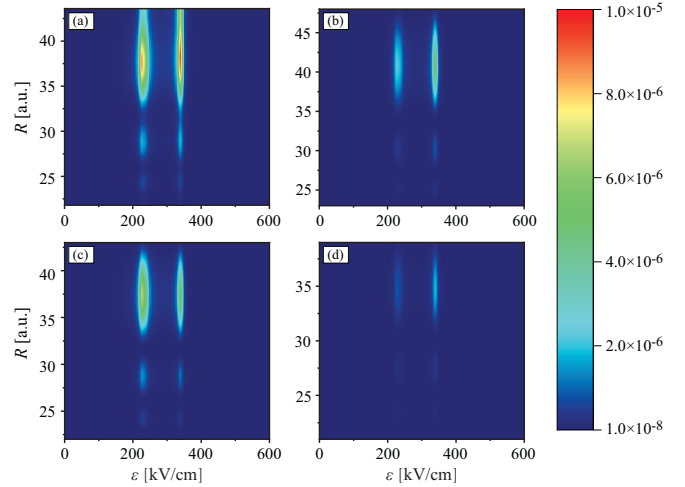


FIG. 5. The short-range probability density of the low-energy scattering state versus electric field and interatomic distance for $\tilde{\beta}_{10} = 0.308064$. (a) The total probability density $|\psi_{\text{total}}(R)|^2$, (b) the s -wave component $|\psi_s(R)|^2$, (c) the p -wave component $|\psi_p(R)|^2$, and (d) the d -wave component $|\psi_d(R)|^2$. The collision energy is $E_{\text{col}} = 0.96 \mu\text{K}$.

density at the selected electric field strength is plotted in Fig. 7. We can see that the short-range probability density is increased by more than two orders of magnitude at $\varepsilon = 309$ kV/cm, where the p -wave bound state is closest to the threshold (see Fig. 4). Moreover, the short-range probability density is always enhanced as long as the bound state becomes closer to the threshold. For example, when ε is 100 kV/cm, the short-range probability density is increased by more than an order of magnitude, as shown in Fig. 7.

D. Heteronuclear alkali-metal collision complexes in electric field

In this section, we calculate the electric-field-induced resonances with realistic potentials for heteronuclear alkali-metal collision complexes in their ground electronic states $X^1\Sigma^+$. The quantum number m is assumed to be zero. The potential-energy curves used in the calculation are shown in Fig. 8(a). The R -dependent permanent dipole moment functions $D(R)$ [37] as shown in Fig. 8(b) are used in the calculation. To

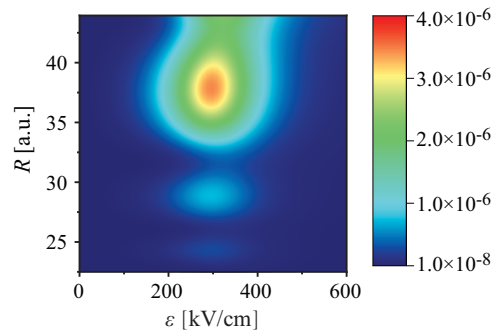


FIG. 6. The short-range probability density of the low-energy scattering state versus electric field and interatomic distance for $\tilde{\beta}_{10} = 0.308045$. The collision energy is $E_{\text{col}} = 0.48 \mu\text{K}$.

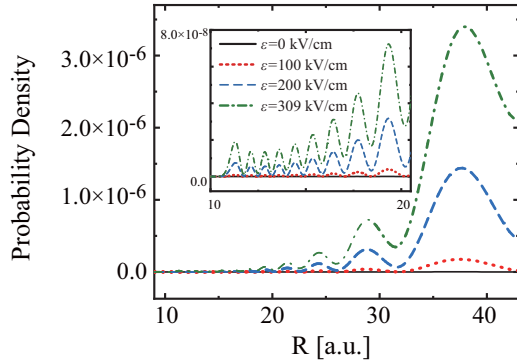


FIG. 7. The short-range probability density of the scattering state at $E_{\text{col}} = 0.48 \mu\text{K}$ as a function of the internuclear distance R at four selected electric-field strengths ε . $\tilde{\beta}_{10}$ is 0.308045. The inset shows the probability density in the range $10 \text{ a.u.} < R < 21 \text{ a.u.}$ clearly.

indicate the relative strength of the permanent dipole moment for a heteronuclear alkali-metal dimer, we summarize the permanent dipole moment $D(R_e)$ at equilibrium distance R_e in

Table I. It is noted that a more recent calculation of $D(R)$ was performed in [53]. In Table I, we also show the van der Waals coefficient C_6 , the scattering length a , the reduced scattering length \tilde{a} , the position of the electric-field-induced resonance, and the partial-wave state which produces the resonance. As shown in Fig. 3(c), more than one resonances can be induced in the electric field. The resonance listed in Table I for each collision complex is the first resonance produced by the $m = 0$ state as the electric field increases.

The resonances in Table I can be classified into three categories according to the partial-wave states which produce the resonances. In Table I, there is no resonance which is caused by a p - or d -wave bound state. This is due to the fact that the least bound p - and d -wave state for all complexes considered in Table I is not close enough to the threshold and cannot cross the threshold in the electric field. For complexes whose \tilde{a} is in the range of $\tilde{a}_d < \tilde{a} < \tilde{a}_p$, such as ${}^6\text{Li}^{39}\text{K}$, ${}^6\text{Li}^{40}\text{K}$, ${}^6\text{Li}^{41}\text{K}$, ${}^7\text{Li}^{85}\text{Rb}$, ${}^7\text{Li}^{87}\text{Rb}$, ${}^{23}\text{Na}^{40}\text{K}$, ${}^{23}\text{Na}^{87}\text{Rb}$, and ${}^{41}\text{K}^{85}\text{Rb}$, there is a d -wave quasibound state at $\varepsilon = 0$, and the first resonance is produced by this d -wave quasibound state crossing the threshold. For the complexes whose \tilde{a} is larger

TABLE I. The permanent dipole moment at equilibrium distance $D(R_e)$, the van der Waals coefficient C_6 , the scattering length a , the reduced scattering length \tilde{a} , the position of the first electric-field-induced resonance, and the partial-wave state which causes the resonance for heteronuclear alkali-metal complexes in the $X^1\Sigma^+$ state are summarized. The references for C_6 and a are given.

	$D(R_e)$ (D)	C_6 (a.u.)	a (a.u.)	\tilde{a} (in units of β_6)	First resonance position (kV/cm)	Partial-wave state
${}^6\text{Li}^{23}\text{Na}$	0.561	1467 [39]	-73 [39]	-1.03	8845	s
${}^7\text{Li}^{23}\text{Na}$	0.561	1467 [39]	5 [39]	0.07	19129	s
${}^6\text{Li}^{39}\text{K}$	3.558	2322 [40]	64.9 [40]	0.80	2920	d
${}^6\text{Li}^{40}\text{K}$	3.558	2322 [40]	52.61 [40]	0.65	2460	d
${}^6\text{Li}^{41}\text{K}$	3.558	2322 [40]	42.75 [40]	0.52	1720	d
${}^7\text{Li}^{39}\text{K}$	3.558	2322 [40]	29.83 [40]	0.35	2130	s
${}^7\text{Li}^{40}\text{K}$	3.558	2322 [40]	14.88 [40]	0.18	1760	s
${}^7\text{Li}^{41}\text{K}$	3.558	2322 [40]	-6.375 [40]	-0.08	1390	s
${}^6\text{Li}^{85}\text{Rb}$	4.168	2550 [41]	7.6 [48]	0.09	1357	s
${}^6\text{Li}^{87}\text{Rb}$	4.168	2550 [41]	0.5 [48]	0.006	1257	s
${}^7\text{Li}^{85}\text{Rb}$	4.168	2550 [41]	60.5 [48]	0.69	1933	d
${}^7\text{Li}^{87}\text{Rb}$	4.168	2550 [41]	53.9 [48]	0.61	1686	d
${}^6\text{Li}^{133}\text{Cs}$	5.520	3065 [42]	24.169 [49]	0.27	1230	s
${}^7\text{Li}^{133}\text{Cs}$	5.520	3065 [42]	39.759 [49]	0.43	1360	s
${}^{23}\text{Na}^{39}\text{K}$	2.760	2439 [43]	331.8 [43]	2.39	1768	p
${}^{23}\text{Na}^{40}\text{K}$	2.760	2439 [43]	66.7 [43]	0.59	1768	d
${}^{23}\text{Na}^{41}\text{K}$	2.760	2439 [43]	3.39 [43]	0.03	1316	s
${}^{23}\text{Na}^{85}\text{Rb}$	3.304	2686 [36]	396 [50]	3.43	1357	p
${}^{23}\text{Na}^{87}\text{Rb}$	3.304	2686 [36]	109 [50]	0.94	1810	d
${}^{23}\text{Na}^{133}\text{Cs}$	4.613	3227 [44]	513 [44]	4.16	925	p
${}^{39}\text{K}^{85}\text{Rb}$	0.615	4299 [45]	33.4 [45]	0.23	3990	s
${}^{39}\text{K}^{87}\text{Rb}$	0.615	4299 [45]	1868 [45]	13.04	5389	p
${}^{40}\text{K}^{85}\text{Rb}$	0.615	4299 [45]	65.8 [45]	0.46	5059	s
${}^{40}\text{K}^{87}\text{Rb}$	0.615	4299 [45]	-111.5 [45]	-0.77	1933	s
${}^{41}\text{K}^{85}\text{Rb}$	0.615	4299 [45]	103.1 [45]	0.71	5430	d
${}^{41}\text{K}^{87}\text{Rb}$	0.615	4299 [45]	7.06 [45]	0.05	3208	s
${}^{39}\text{K}^{133}\text{Cs}$	1.906	5159 [46]	-18.4 [46]	-0.12	946	s
${}^{40}\text{K}^{133}\text{Cs}$	1.906	5159 [46]	-51.5 [46]	-0.33	781	s
${}^{41}\text{K}^{133}\text{Cs}$	1.906	5159 [46]	-72.8 [46]	-0.47	740	s
${}^{85}\text{Rb}^{133}\text{Cs}$	1.238	5694 [47]	585.6 [51]	3.23	1768	p
${}^{87}\text{Rb}^{133}\text{Cs}$	1.238	5694 [47]	997 [52]	5.49	1851	p

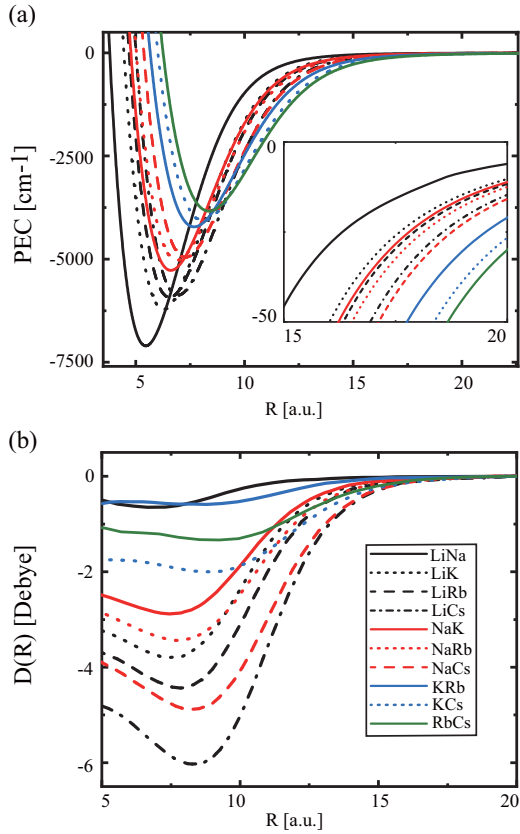


FIG. 8. (a) The potential-energy curves (PECs) of the heteronuclear alkali-metal molecules in the $X^1\Sigma^+$ state as a function of internuclear distance R . The inset shows the PEC in the range $15 \text{ a.u.} < R < 20 \text{ a.u.}$. The black lines denote the Li compounds (solid line for LiNa [39], dotted line for LiK [40], dashed line for LiRb [41], dot-dashed line for LiCs [42]). The red lines denote the Na compounds (solid line for NaK [43], dotted line for NaRb [36], dashed line for NaCs [44]). The blue lines denote the K compounds (solid line for KRb [45], dotted line for KCs [46]). The solid green line is for RbCs [47]. (b) The R -dependent permanent dipole moments $D(R)$ adopted from [37]. The long-range part of $D(R)$ is fitted to be exponentially decaying. The same line types and color code as in (a) are used for the collision complexes.

than \tilde{a}_p , such as $^{23}\text{Na}^{39}\text{K}$, $^{23}\text{Na}^{85}\text{Rb}$, $^{23}\text{Na}^{133}\text{Cs}$, $^{39}\text{K}^{87}\text{Rb}$, $^{85}\text{Rb}^{133}\text{Cs}$, and $^{87}\text{Rb}^{133}\text{Cs}$, there is a p -wave quasibound state at $\varepsilon = 0$, and the first resonance is produced by this p -wave quasibound state crossing the threshold. For the remaining complexes in Table I, \tilde{a} is smaller than \tilde{a}_d , and the first resonance is caused by the s -wave virtual state crossing the threshold.

The electric field couples different partial-wave states via the permanent dipole moment. Thus, the permanent dipole moment $D(R)$ is one important factor affecting the position of the first resonance. In general, the smaller the permanent dipole moment is, the stronger the electric field required to induce the first resonance is, as shown in Table I. For example, the permanent dipole moment of LiNa is the smallest among the heteronuclear alkali-metal complexes. Hence, the first resonance of $^6\text{Li}^{23}\text{Na}$ and $^7\text{Li}^{23}\text{Na}$ appears at 8845

and 19129 kV/cm, respectively, which are the two strongest electric fields in Table I.

The position of the bound or quasibound (virtual) states at $\varepsilon = 0$ is another important factor affecting the position of the resonance. The permanent dipole moment of the KCs complex is smaller than that of the LiCs complex. Nevertheless, it is shown in Table I that the resonance of the KCs complex occurs at lower electric field than that of LiCs. The reason is that, for KCs, the scattering length \tilde{a} is negative and there is a virtual state close to the threshold. As the scattering length \tilde{a} is more negative, the virtual state is closer to the threshold, and correspondingly, the resonance occurs at lower electric field. This explains the variation of the resonance positions for the three KCs isotopes ($^{39}\text{K}^{133}\text{Cs}$, $^{40}\text{K}^{133}\text{Cs}$, and $^{41}\text{K}^{133}\text{Cs}$) in Table I. The variation of the resonance positions for three ^6LiK isotopes ($^6\text{Li}^{39}\text{K}$, $^6\text{Li}^{40}\text{K}$, and $^6\text{Li}^{41}\text{K}$) in Table I can be interpreted in a similar way. For the three ^6LiK isotopes, \tilde{a} is larger than \tilde{a}_d , and there is a d -wave quasibound state above the threshold. The \tilde{a} for $^6\text{Li}^{41}\text{K}$ is closest to \tilde{a}_d , and hence, the quasibound state is closest to the threshold. As a consequence, the resonance for $^6\text{Li}^{41}\text{K}$ is induced at the lowest electric field among the three isotopes. In general, resonances at low electric field are expected if there is a bound or quasibound (virtual) state close to the threshold. The scattering length is an indication of the position of the bound or quasibound (virtual) state and can be used to guide the search for a system which possesses resonance at low electric field.

It is worth noting that the scattering length \tilde{a} of the $^{23}\text{Na}^{87}\text{Rb}$ complex in the $X^1\Sigma^+$ state is smaller than \tilde{a}_p and close to \tilde{a}_p . Therefore, there is a p -wave bound state near the threshold in the $^{23}\text{Na}^{87}\text{Rb}$ molecule. When the external electric field is applied, the energy of this p -wave bound state initially increases and then decreases. At nearly 300 kV/cm, the energy of this p -wave state reaches its maximum, and the state is closest to the threshold. Although this p -wave state does not cross the threshold and no resonance is induced, the short-range probability density of the low-energy scattering states can be enhanced by two orders there. The $^7\text{Li}^{133}\text{Cs}$ complex has a similar property, the scattering length \tilde{a} of which is close to \tilde{a}_d .

E. The resonances produced by the states with $m \neq 0$

In an electric field, the l partial-wave bound state splits into $l + 1$ levels due to the Stark effect [54]. The Stark levels are identified by the absolute value of the magnetic quantum number $|m|$. In the previous discussion, we considered the cases with $m = 0$. In the following, we investigate the variation of the Stark levels with $m \neq 0$ for p - and d -wave states and the resonances induced by these states. In this section, the prototype model is used, and the interatomic interaction is described by the LJ potential.

The variation of the $|m| = 1$ Stark level for a p -wave bound state in the electric field is shown by the red dotted line in Fig. 9(a). In the calculation $\tilde{\beta}_{10}$ is 0.308064 (point 4 in Fig. 1). It is shown in Fig. 9(a) that the Stark level with $l = 1$, $|m| = 1$ decreases as the electric field increases and does not produce a resonance in the electric field. In fact, all the Stark levels with $|m| = l$ decrease monotonically in the electric field [54]. For comparison, the $m = 0$ component of the same p -wave bound

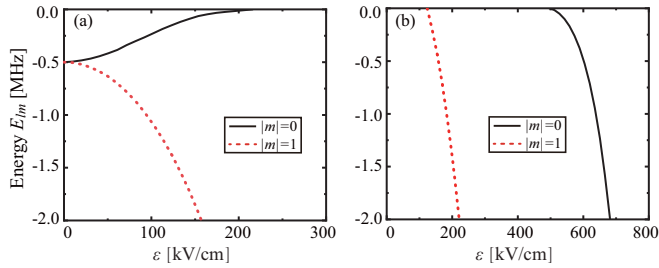


FIG. 9. The variation of the Stark levels for a p -wave bound state as a function of the electric field. In the absence of the electric field, the collision complex has (a) a p -wave bound state with energy $E = -0.5$ MHz or (b) a p -wave quasibound state with energy $E = 0.5$ MHz. Black solid line, $m = 0$; red dotted line, $|m| = 1$.

state, previously shown in Fig. 3(c), is also shown by the black solid line in Fig. 9(a).

For the case in which there is a p -wave quasibound state with $E_p = 0.5$ MHz at $\varepsilon = 0$ (point 5 in Fig. 1), the $|m| = 1$ Stark level induces a zero-energy resonance at $\varepsilon = 123$ kV/cm, as shown by the red dotted line in Fig. 9(b). The $m = 0$ Stark level of the same p -wave state, previously shown in Fig. 3(d), is shown by the black solid line in Fig. 9(b). One can see that, for this case, the $|m| = 1$ Stark level induces a resonance at lower electric field.

Now we examine the case that has a d -wave bound state close to the threshold (point 2 in Fig. 1). The variation of the Stark levels for the d -wave bound state in an electric field is shown in Fig. 10. The Stark level with $l = 2$, $m = 0$ is shown by a black solid line and was discussed in Sec. III B. The Stark level with $l = 2$, $|m| = 1$ is shown by the red dotted line. Away from the threshold, Ref. [54] showed that this Stark level increases in the low-electric-field region and decreases in the strong-electric-field region. Close to the threshold, we found that it decreases monotonically with the increase of electric field, as shown in Fig. 10. The Stark level with $l = 2$, $|m| = 2$ is shown by the blue dashed line. This level decreases monotonically as expected for a level with $|m| = l$. Hence, the d -wave bound state with $|m| = 1$ and 2

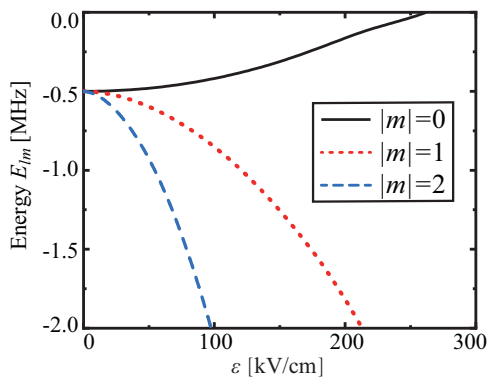


FIG. 10. The variation of the Stark levels for a d -wave bound state as a function of the electric field. In the absence of the electric field, the collision complex has a d -wave bound state with energy $E = -0.5$ MHz. Black solid line, $m = 0$; red dotted line, $|m| = 1$; blue dashed line, $|m| = 2$.

cannot cross the threshold in the electric field. When there is a d -wave quasibound state close to the threshold at $\varepsilon = 0$, all its Stark levels with $|m| = 0, 1$, and 2 can cross the threshold and induce resonances with the increase of electric field. Similar to the p -wave case, the resonance occurs at lower electric field as $|m|$ increases.

Briefly, the s -, p -, and d -wave bound states can cross the threshold and produce the resonance in the electric field only if their magnetic quantum number m equals zero. However, the s -, p -, and d -wave quasibound states with any m can produce the resonance in the electric field, and the resonance positions become larger as $|m|$ decreases.

IV. CONCLUSION

We have investigated the variation of the heteronuclear two-body bound state in an external electric field. We calculate the bound states close to the threshold, which are closely related to the ultracold atomic collision. Due to the interaction between the permanent dipole moment of the heteronuclear dimer and the electric field, the energy of the s -wave bound state decreases monotonically. Hence, the s -wave bound state below the threshold cannot cross the threshold and produce a resonance in the electric field. Instead, an s -wave virtual state can cause a zero-energy resonance with the increase of the electric field. As the s -wave virtual state is closer to the threshold in the absence of the electric field, the resonance occurs at lower electric field. The p - and d -wave states split in the electric field due to the Stark effect. For p - and d -wave bound states, the Stark level with magnetic quantum number $m = 0$ first increases and then decreases as the electric field increases. If the p - or d -wave bound state is close enough to the threshold, the $m = 0$ Stark level can cross the threshold and causes a resonance. Close to the threshold, all the $m \neq 0$ Stark levels of the p - and d -wave bound states decrease monotonically with the increase of electric field and cannot cross the threshold and produce a resonance in the electric field. For the p - or d -wave quasibound state, all the Stark levels can cross the threshold, and the Stark level with a larger $|m|$ produces resonances at lower electric field. Due to the relation between the scattering length and the energy of the l -wave bound or quasibound (virtual for s wave) state [32], the scattering length can be used to identify and classify the electric-field-induced resonance, which is demonstrated by calculating the first electric-field-induced resonance for all the heteronuclear alkali-metal collision complexes in their ground electronic state $X^1\Sigma^+$.

For a collision complex having a p - or d -wave bound state near but not very close to the threshold, the $m = 0$ Stark level of such a state moves towards the threshold but never crosses it with the increase of the electric field. We find that the short-range probability density of the low-energy scattering state is enhanced by orders of magnitude as this $m = 0$ Stark level approaches the threshold. It is expected that the photoassociation rate will be enhanced as well in such a case, although there is no electric-field-induced resonance.

In this work, we do not consider the hyperfine structures of the atoms, and all the electric-field-induced resonances are shape resonances. In the future, we will consider hyperfine structures of atoms and investigate the electric-field-induced

Feshbach resonance when there is an l -wave bound or quasisubbound state near the threshold of the entrance channel. In addition, the impact of the electric-field-induced resonance on the wave-packet dynamics triggered by intense laser pulses was investigated recently [55]. In this work, a resonance is classified according to the bound state which induces the resonance. It will be interesting to find out if different types of resonances will result in distinguishable dynamics in laser pulses.

ACKNOWLEDGMENTS

This work is supported by the Fundamental Research Funds for the Central Universities DUT19LK35, the Program of the State Key Laboratory of Quantum Optics and Quantum Optics Devices (No. KF201814), the National Key R&D Program of China (No. 2018YFA0306503), and the National Natural Science Foundation of China under Grant No. 11274056.

- [1] K.-K. Ni, S. Ospelkaus, M. H. G. de Miranda, A. Pe'er, B. Neyenhuis, J. J. Zirbel, S. Kotochigova, P. S. Julienne, D. S. Jin, and J. Ye, *Science* **322**, 231 (2008)
- [2] P. K. Molony, P. D. Gregory, Z. Ji, B. Lu, M. P. Köppinger, C. R. Le Sueur, C. L. Blackley, J. M. Hutson, and S. L. Cornish, *Phys. Rev. Lett.* **113**, 255301 (2014).
- [3] T. Takekoshi, L. Reichsöllner, A. Schindewolf, J. M. Hutson, C. R. Le Sueur, O. Dulieu, F. Ferlaino, R. Grimm, and H.-C. Nägerl, *Phys. Rev. Lett.* **113**, 205301 (2014).
- [4] M. Guo, B. Zhu, B. Lu, X. Ye, F. Wang, R. Vexiau, N. Bouloufa-Maafa, G. Quémener, O. Dulieu, and D. Wang, *Phys. Rev. Lett.* **116**, 205303 (2016).
- [5] L. De Marco, G. Valtolina, K. Matsuda, W. G. Tobias, J. P. Covey, and J. Ye, *Science* **363**, 853 (2019).
- [6] J. Ullmanis, S. Häfner, E. D. Kuhnle, and M. Weidemüller, *Natl. Sci. Rev.* **3**, 174 (2016).
- [7] X. C. Yao, H. Z. Chen, Y. P. Wu, X. P. Liu, X. Q. Wang, X. Jiang, Y. Deng, Y. A. Chen, and J. W. Pan, *Phys. Rev. Lett.* **117**, 145301 (2016).
- [8] G. Semeghini, G. Ferioli, L. Masi, C. Mazzinghi, L. Wolswijk, F. Minardi, M. Modugno, G. Modugno, M. Inguscio, and M. Fattori, *Phys. Rev. Lett.* **120**, 235301 (2018).
- [9] E. Fava, T. Bienaimé, C. Mordini, G. Colzi, C. Qu, S. Stringari, G. Lamporesi, and G. Ferrari, *Phys. Rev. Lett.* **120**, 170401 (2018).
- [10] X.-Y. Luo, Y.-Q. Zou, L.-N. Wu, Q. Liu, M.-F. Han, M. K. Tey, and L. You, *Science* **355**, 620 (2017).
- [11] R. González-Férez and P. Schmelcher, *Phys. Rev. A* **69**, 023402 (2004).
- [12] R. González-Férez and P. Schmelcher, *Phys. Rev. A* **71**, 033416 (2005).
- [13] R. González-Férez and P. Schmelcher, *Europhys. Lett.* **72**, 555 (2005).
- [14] R. González-Férez, M. Mayle, and P. Schmelcher, *Chem. Phys.* **329**, 203 (2006).
- [15] M. Mayle, R. González-Férez, and P. Schmelcher, *Phys. Rev. A* **75**, 013421 (2007).
- [16] R. González-Férez, M. Weidemüller, and P. Schmelcher, *Phys. Rev. A* **76**, 023402 (2007).
- [17] C. Ticknor and J. L. Bohn, *Phys. Rev. A* **72**, 032717 (2005)
- [18] D. Chakraborty, J. Hazra, and B. Deb, *J. Phys. B* **44**, 095201 (2011).
- [19] D. Chakraborty and B. Deb, *AIP Adv.* **4**, 017134 (2014).
- [20] R. V. Krems, *Phys. Rev. Lett.* **96**, 123202 (2006).
- [21] Z. Li and R. V. Krems, *Phys. Rev. A* **75**, 032709 (2007).
- [22] L.-H. Li, J.-L. Li, G.-R. Wang, and S.-L. Cong, *J. Chem. Phys.* **150**, 064310 (2019).
- [23] T. Xie, G.-R. Wang, W. Zhang, Y. Huang, and S.-L. Cong, *Phys. Rev. A* **84**, 032712 (2011).
- [24] T. Xie, G.-R. Wang, W. Zhang, Y. Huang, and S.-L. Cong, *Phys. Rev. A* **86**, 032713 (2012).
- [25] C. Chin, R. Grimm, P. Julienne, and E. Tiesinga, *Rev. Mod. Phys.* **82**, 1225 (2010).
- [26] B. Marcellis, E. G. M. van Kempen, B. J. Verhaar, and S. J. J. M. F. Kokkelmans, *Phys. Rev. A* **70**, 012701 (2004).
- [27] M. Marinescu and L. You, *Phys. Rev. Lett.* **81**, 4596 (1998).
- [28] B. Deb and L. You, *Phys. Rev. A* **64**, 022717 (2001).
- [29] R. González-Férez and P. Schmelcher, *New J. Phys.* **11**, 055013 (2009).
- [30] M. Iñarrea, J. P. Salas, R. González-Férez, and P. Schmelcher, *Phys. Lett. A* **374**, 457 (2010).
- [31] K. Willner, O. Dulieu, and F. Masnou-Seeuws, *J. Chem. Phys.* **120**, 548 (2004).
- [32] B. Gao, *Phys. Rev. A* **62**, 050702(R) (2000).
- [33] B. Gao, *J. Phys. B* **36**, 2111 (2003).
- [34] B. Gao, *Phys. Rev. A* **80**, 012702 (2009).
- [35] Y. Cui, C. Shen, M. Deng, S. Dong, C. Chen, R. Lu, B. Gao, M. K. Tey, and L. You, *Phys. Rev. Lett.* **119**, 203402 (2017).
- [36] F. Wang, D. Xiong, X. Li, D. Wang, and E. Tiemann, *Phys. Rev. A* **87**, 050702(R) (2013).
- [37] M. Aymar and O. Dulieu, *J. Chem. Phys.* **122**, 204302 (2005).
- [38] K. von Meyenn, *Z. Phys.* **231**, 154 (1970).
- [39] M. Steinke, H. Knöckel, and E. Tiemann, *Phys. Rev. A* **85**, 042720 (2012).
- [40] E. Tiemann, H. Knöckel, P. Kowalczyk, W. Jastrzebski, A. Pashov, H. Salami, and A. J. Ross, *Phys. Rev. A* **79**, 042716 (2009).
- [41] M. Ivanova, A. Stein, A. Pashov, H. Knöckel, and E. Tiemann, *J. Chem. Phys.* **134**, 024321 (2011).
- [42] P. Staunum, A. Pashov, H. Knöckel, and E. Tiemann, *Phys. Rev. A* **75**, 042513 (2007).
- [43] M.-J. Zhu, H. Yang, L. Liu, D.-C. Zhang, Y.-X. Liu, J. Nan, J. Rui, B. Zhao, J.-W. Pan, and E. Tiemann, *Phys. Rev. A* **96**, 062705 (2017).
- [44] O. Docenko, M. Tamanis, J. Zaharova, R. Ferber, A. Pashov, H. Knöckel, and E. Tiemann, *J. Phys. B* **39**, S929 (2006).
- [45] A. Pashov, O. Docenko, M. Tamanis, R. Ferber, H. Knöckel, and E. Tiemann, *Phys. Rev. A* **76**, 022511 (2007).
- [46] R. Ferber, O. Nikolayeva, M. Tamanis, H. Knöckel, and E. Tiemann, *Phys. Rev. A* **88**, 012516 (2013).
- [47] T. Takekoshi, M. Debatin, R. Rameshan, F. Ferlaino, R. Grimm, H.-C. Nägerl, C. R. Le Sueur, J. M. Hutson, P. S. Julienne, S. Kotochigova, and E. Tiemann, *Phys. Rev. A* **85**, 032506 (2012).
- [48] C. Marzok, B. Deh, C. Zimmermann, P. W. Courteille, E. Tiemann, Y. V. Vanne, and A. Saenz, *Phys. Rev. A* **79**, 012717 (2009).

- [49] A. L. M. Zanelatto, E. M. S. Ribeiro, and R. d. J. Napolitano, *J. Chem. Phys.* **123**, 014311 (2005).
- [50] A. Pashov, O. Docenko, M. Tamanis, R. Ferber, H. Knöeckel, and E. Tiemann, *Phys. Rev. A* **72**, 062505 (2005).
- [51] H.-W. Cho, D. J. McCarron, M. P. Köppinger, D. L. Jenkin, K. L. Butler, P. S. Julienne, C. L. Blackley, C. R. Le Sueur, J. M. Hutson, and S. L. Cornish, *Phys. Rev. A* **87**, 010703(R) (2013).
- [52] M. P. Köppinger, D. J. McCarron, D. L. Jenkin, P. K. Molony, H.-W. Cho, S. L. Cornish, C. R. Le Sueur, C. L. Blackley, and J. M. Hutson, *Phys. Rev. A* **89**, 033604 (2014).
- [53] D. A. Fedorov, A. Derevianko, and S. A. Varganov, *J. Chem. Phys.* **140**, 184315 (2014).
- [54] K. Larsson and P. O. Fröman, *Philos. Trans. R. Soc. London, Ser. A* **347**, 23 (1994).
- [55] Q. Guan and D. Blume, *Phys. Rev. A* **99**, 033416 (2019).